Tunnelling and Underground Space Technology 125 (2022) 104499

Contents lists available at ScienceDirect

Tunnelling and Underground Space Technology incorporating Trenchless Technology Research

journal homepage: www.elsevier.com/locate/tust

Early-stage assessment of structural damage caused by braced excavations: Uncertainty quantification and a probabilistic analysis approach

Jinyan Zhao [a], Stefan Ritter [b], Matthew J. DeJong [c,*]

[a] Department of Civil and Environmental Engineering, University of California, Berkeley, CA 94720, United States
[b] Onshore Foundations, Norwegian Geotechnical Institute, Sognsveien 72, 08555 Oslo, Norway
[c] Department of Civil and Environmental Engineering, University of California, Berkeley, CA 94720, United States

ARTICLE INFO

Keywords:
Deep excavation
Building damage
Soil-structure-interaction
Uncertainty quantification
Global sensitivity analysis

ABSTRACT

Current early stage assessment methods for deep excavation induced structural damage have large uncertainty due to modeling idealizations (simplification in analyses) and ignorance (incompleteness of information). This paper implements an elastoplastic two-stage solution of soil-structure-interaction to predict building response to adjacent deep excavations with braced supports. This soil-structure-interaction solution is then used to study the uncertainty in two case studies. A global sensitivity analysis is conducted, which indicates that the prediction of ground movement profiles is the major source of uncertainty in early stage building damage assessment. The uncertainty due to ignorance and idealizations related to structural analysis models also contribute significantly when target buildings are modeled as equivalent beams. However, the use of a 2-dimensional elastic frame structural model, in lieu of an equivalent beam, considerably reduces the assessment uncertainty. Considering the existence of uncertainty, a probabilistic analysis approach is proposed to quantify the uncertainty when predicting potential building damage due to excavation-induced subsidence. A computer program called Uncertainty Quantification in Excavation-Structure Interaction (UQESI) is developed to implement this probabilistic analysis approach.

1. Introduction

In major deep excavation projects, there are often many buildings influenced by construction activities. It is a challenge to assess all of these buildings with detailed analysis to identify potential damage. To address this challenge, a staged approach by Mair et al. (1996) is commonly adopted which consists of three stages: preliminary assessment, second stage assessment and detailed evaluation. In the preliminary assessment stage, a settlement contour is computed and the buildings with a predicted settlement of less than 10 mm and a predicted slope of less than 1:500 are considered to have a negligible risk of damage. Otherwise, buildings are qualified for a second stage assessment, in which some engineering demand parameters (e.g., distortion, deflection ratio and tensile strain) are calculated. A potential damage category is assigned to each building and the buildings with severe damage potential are required to be evaluated in detail in a third assessment stage.

The current second stage assessment methods consist of many simplified models and empirical equations, which often lead to unreliable and sometimes overly conservative damage evaluation results. Moreover, because no comprehensive survey is done in the second assessment stage, details of structure layouts and material properties are often unavailable. Consequently, many assumptions and approximations are made in the analyses, which introduce large uncertainty to building damage evaluations. This paper aims to study the uncertainty in the second assessment stage of brace-supported deep excavations and proposes suggestions on optimal trade-offs between analysis complexity and prediction accuracy. Current second stage assessment can be divided into three components (Schuster et al., 2009): (1) lateral and vertical ground displacement profiles are determined; (2) engineering demand parameters are estimated based on various soil-structure interaction (SSI) assumptions; (3) building damage categories are determined according to the engineering demand parameters. In this paper, these three components are implemented with a numerical analysis framework (extended from Franza and DeJong (2019)) which considers elastoplastic SSI effects. Two case studies of deep excavation in urban areas are explored. Uncertainty and sensitivity analyses are conducted for the case studies and suggestions to reduce damage

* Corresponding author.
E-mail address: dejong@berkeley.edu (M.J. DeJong).

https://doi.org/10.1016/j.tust.2022.104499
Received 21 December 2020; Received in revised form 31 March 2022; Accepted 1 April 2022
Available online 10 April 2022

assessment uncertainty are provided. A probabilistic analysis approach is then proposed to quantify the uncertainties caused by the approximations and simplifications in analyses, so that a confidence level of the predicted building damage can be provided. A computer program called Uncertainty Quantification in Excavation Structure Interaction (UQESI), which enables efficient SSI analysis and yields uncertainty quantification and sensitivity analysis, is proposed.

2. Background

2.1. Estimation of greenfield ground displacement profile

The first component in the second stage assessment is to determine greenfield ground displacement profiles, which describe the excavation-induced ground movements when the effect of surface buildings is ignored. For braced excavations, a concave-shaped ground displacement profile is usually adopted. Hsieh and Ou (1998) proposed a method to estimate the vertical ground settlement profile by: 1) predict the maximum lateral wall deflection (δ_{hm}) with numerical methods (e.g. finite element or beam on elastic foundation methods); 2) estimate the maximum vertical ground surface settlement (δ_{vm}) from empirical relationships with δ_{hm}; 3) calculate the surface settlement at various distances (d) behind the wall according to Eq. (1). Hsieh and Ou (1998)'s ground profile is derived based on a regression analysis of 10 case studies, and might be biased due to the small sample size.

Kung et al. (2007) therefore extended the regression analysis by including more case studies and a suite of artificial scenarios analyzed with the finite element method. The vertical ground displacement profile revised by Kung et al. (2007) is expressed in Eq. (2). Based on regression analysis, Kung et al. (2007) also proposed empirical equations to estimate the maximum horizontal wall deflection (δ_{hm}) and the deformation ratio (R_v) between δ_{vm} and δ_{hm} (i.e., $R_v = \frac{\delta_{vm}}{\delta_{hm}}$). The empirical equations (also referred to as the KJHH model) estimate δ_{hm} and δ_{vm} based on the dimensions of the excavation system, the soil shear strength, the soil elastic modulus, the soil effective stress, the support system stiffness and the depth to hard stratum. A comparison of Hsieh and Ou (1998) and Kung et al. (2007)'s settlement profile is shown in Fig. 2a.

Schuster et al. (2009) studied the lateral displacement induced by deep excavation using the same finite element model as developed by Kung et al. (2007). A horizontal ground displacement (δ_l) profile (Eq. (3)) and empirical equations to estimate the lateral deformation ratio ($R_l = \frac{\delta_{lm}}{\delta_{hm}}$) were proposed. The parameters used to estimate R_l are identical to the parameters used in the KJHH model, and the empirical equations are referred to as the KSJH model.

$$\begin{aligned}
\delta_v(d) &= \left(\frac{d}{H_e} + 0.5\right)\delta_{vm} && 0.0 < \frac{d}{H_e} \le 0.5 \\
\delta_v(d) &= \left(-0.6\frac{d}{H_e} + 1.3\right)\delta_{vm} && 0.5 < \frac{d}{H_e} \le 2.0 \\
\delta_v(d) &= \left(-0.05\frac{d}{H_e} + 0.2\right)\delta_{vm} && 2.0 < \frac{d}{H_e} \le 4.0
\end{aligned} \tag{1}$$

$$\begin{aligned}
\delta_v(d) &= \left(1.6\frac{d}{H_e} + 0.2\right)\delta_{vm} && 0.0 < \frac{d}{H_e} \le 0.5 \\
\delta_v(d) &= \left(-0.6\frac{d}{H_e} + 1.3\right)\delta_{vm} && 0.5 < \frac{d}{H_e} \le 2.0 \\
\delta_v(d) &= \left(-0.05\frac{d}{H_e} + 0.2\right)\delta_{vm} && 2.0 < \frac{d}{H_e} \le 4.0
\end{aligned} \tag{2}$$

$$\begin{aligned}
\delta_l(d) &= \left(0.8\frac{d}{H_e} + 0.2\right)\delta_{lm} && 0.0 < \frac{d}{H_e} \le 1.0 \\
\delta_l(d) &= \left(-0.4\frac{d}{H_e} + 1.4\right)\delta_{lm} && 1.0 < \frac{d}{H_e} \le 2.5 \\
\delta_l(d) &= \left(-0.16\frac{d}{H_e} + 0.8\right)\delta_{lm} && 2.5 < \frac{d}{H_e} \le 5.0
\end{aligned} \tag{3}$$

The KJHH and KSJH models are considered as an appropriate method to estimate ground displacement profiles for the early assessment stage because δ_{hm}, δ_v and δ_l can be approximated without any complex modeling of the excavation system. This ensures a simplified analysis procedure, although some uncertainty is introduced due to the variance and possible bias of the regression analyses. The implementation of the KJHH and KSJH models to assess SSI mechanisms and their respective uncertainties are discussed in later sections.

2.2. Estimation of structure deformation

Because of soil-structure interaction effects, the displaced shape of the soil at the base of a surface structure is usually different from that of typically measured greenfield ground displacements. To quantify the effect of structural stiffness on estimating structural deformation, two different approaches are often adopted: 1) the relative stiffness approach and 2) the soil-structure-interaction (SSI) approach.

In the relative stiffness approach, the differences between building response and greenfield ground displacement are often described with modification factors for the deflection ratio and horizontal strain in both the sagging and hogging region. Many authors (e.g., Potts and Addenbrooke, 1997; Dimmock and Mair, ,2008; Franzius et al., 2006) proposed variants of the relative stiffness approach to estimate tunneling-induced settlement based on design charts of relative stiffness factors and modification factors. Mair (2013) also studied the effects of deep excavations on surface structures and proposed a bending stiffness factor and corresponding design charts to estimate modification factors. In practice, the relative stiffness approach can be easily implemented but only provides approximate solutions. Additionally, there is often a large discrepancy between the analysis results with different relative stiffness factors, which subsequently cause large uncertainty in the estimation of building deformation (e.g., Giardina et al., 2018).

Another method to estimate building deformation is to analyze the soil-structure-interaction explicitly. Franza and DeJong (2019) proposed an elastoplastic solution, in which the interface between soil and structure is modeled as rigid-perfectly plastic elements (also called plastic sliders) with upper and lower limit forces (See Fig. 1). The soil structure interface is discretized and sliders are applied both vertically and horizontally at the nodes. The soil is modeled as a homogeneous

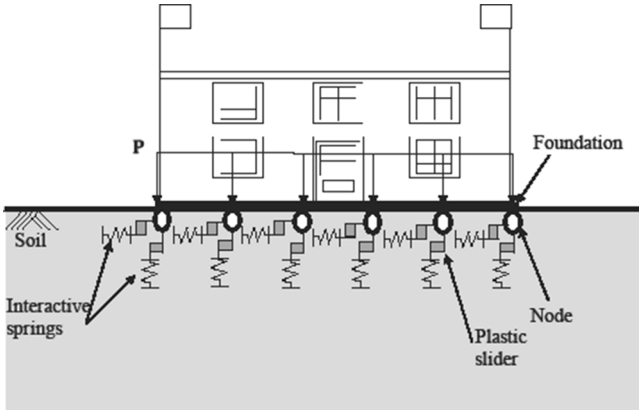

Fig. 1. Sketch of the elastoplastic soil-structure interaction model (after Franza and DeJong (2019)).

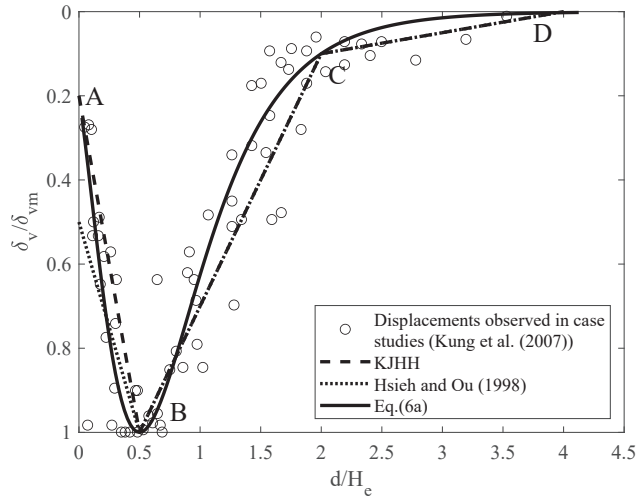

(a) Vertical ground displacement profile

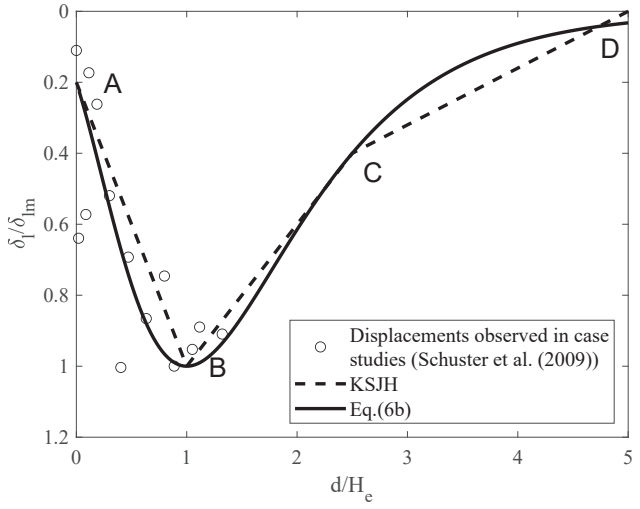

(b) lateral ground displacement profile

Fig. 2. The proposed surface ground movement profiles.

half-space continuum represented by coupled interactive springs. Gaps and slippage following the Coulomb friction model between soil and structure can be simulated with the plastic sliders by setting a zero upper limit force and a horizontal limit force proportional to the vertical stress in the sliders. The building displacement (**u**) at each node can be solved with an equilibrium equation (Eq. (4)), where **S** is building stiffness, $\mathbf{K}^*$ is the stiffness matrix of soil, **P** is the external loading applied at the foundation, $\mathbf{u}^{ip}$ is the plastic displacement of the sliders, Λ^* is the soil flexibility matrix without the main diagonal and $\mathbf{u}^{cat}$ is the greenfield ground displacement induced by excavation. The plastic property of sliders are governed by Eq. 4b and Eq. 4c, where $f_{i,low}$ and $f_{i,up}$ are upper and lower limits of the vertical force in sliders, μ is the friction coefficient at the interface of soil and structure and i and j are respectively the vertical and horizontal degree of freedom. The soil stiffness matrices $\mathbf{K}^*$ and $\mathbf{\Lambda}^*$ can be derived from the Mindlin's solution given by Vaziri et al. (1982). The structure stiffness **S** can be determined with analytical solutions or finite element formulations. Because Eq. (4) is nonlinear without closed-form solutions, it is solved with the iterative algorithm proposed by Klar et al. (2007). The analysis result of Eq. (4) has been compared with centrifuge tests and confirmed to be reliable by Franza and DeJong (2019) and Franza et al. (2020b). Elkayam and Klar (2019) also validated this elastoplastic formulation with a finite difference model of the soil continuum. Besides this elastoplastic solution, there are other SSI analysis methods involving full scale finite element interface modeling and more rigorous soil constitutive models (e.g., Giardina et al., 2013, 2020; Amorosi et al., 2014; Fargnoli et al., 2015; Boldini et al., 2018; Yiu et al., 2017). However, such complex models are generally not practicable in the second stage assessment of large urban infrastructure projects and therefore not considered in this paper.

$$(\mathbf{S}+\mathbf{K}^*)\mathbf{u}=\mathbf{P}+\mathbf{K}^*\mathbf{u}^{cat}+\mathbf{K}^*\mathbf{\Lambda}^*(\mathbf{P}-\mathbf{Su})+\mathbf{K}^*\mathbf{u}^{ip} \quad \text{subject to :} \tag{4a}$$

$$f_{i,low}\le(\mathbf{P}-\mathbf{Su})_i\le f_{i,up} \tag{4b}$$

$$|(\mathbf{P}-\mathbf{Su})_j|\le\mu(\mathbf{P}-\mathbf{Su})_i \tag{4c}$$

2.3. Structure damage evaluation methods

After the building deformation is estimated, a measure of potential damage in the building is needed. When each building element are not evaluated in detail and only the deformation mode, construction types and some other simple features are taken into consideration, semi-empirical methods can be adopted to evaluate the structural damage (e.g., Burland et al., 1978; Boscardin and Cording, 1989; Son and Cording, 2005). Semi-empirical methods typically depend on crucial simplifications of structure and boundary conditions, and can only provide a rough estimation of building damage. The most widely used semi-empirical methods and some of their limitations are reviewed in the Appendix 1.

When prediction methods can provide sufficiently specific information, such as building internal forces or strains, damage assessment approaches which are more detailed than semi-empirical methods can be adopted. Franza et al. (2020b) proposed a direct strain based approach where no assumptions of deflection ratio or angular distortion are needed. The building strains are directly calculated from measured deformations of the building or internal forces calculated from the equivalent beam model using Eq. (5), where χ_m is the beam curvature, γ_m is the beam engineering shear strain, $\varepsilon_{axis,m}$ is the beam axis strain, and N_m, V_m, M_m are the internal axial force, shear force and bending moment computed from numerical analysis; k and c are the shear correction factor and the average shear stress correction factor, which depend on the geometry of building cross-section, t is the distance between neutral axis and extreme fiber and s is the vertical distance between the neutral axis and the fibre where ε_{dt} is calculated. The larger of ε_{bt} and ε_{dt} is taken as ε_{crit} and compared with the classification criterion proposed by Boscardin and Cording (1989) (See Table 1). This direct strain based approach uses an isotropic equivalent beam to model an entire building, therefore only a damage level of the entire building can be estimated. If the damage condition of some building elements or the locations of damages are desired, more detailed models have to be adopted. The detailed models should contain both structural and non-structural elements (e.g., infill walls). One such detailed damage assessment method for frame structures is proposed in section 3.3.

Table 1
Relationship between category of damage and critical tensile strain (ε_{crit}) (after Boscardin and Cording (1989), the values in bracket are suggested by Son and Cording (2005)).

Category of damage	Nominal degree of severity	Critical tensile strain (ε_{crit})(%)
0	Negligible	0–0.05
1	Very slight	0.05–0.075
2	Slight	0.075–0.15 (0.075–0.167)
3	Moderate	0.15–0.3 (0.167–0.333)
4 to 5	Severe to very severe	>0.3 (>0.333)

$$\varepsilon_b = \chi_m t = \frac{M_m t}{EI}\varepsilon'_b = \chi_m s = \frac{M_m s}{EI}\varepsilon_d = \frac{c\gamma_m}{2} = \frac{cV_m}{s\kappa AG}\varepsilon_h = \varepsilon_{axis,m} = \frac{N_m}{EA}$$
$$\varepsilon_{bt} = \varepsilon_b + \varepsilon_h\varepsilon_{dt} = (\varepsilon'_b + \varepsilon_h)\left(\frac{1-\nu}{2}\right) + \sqrt{(\varepsilon'_b + \varepsilon_h)^2\left(\frac{1+\nu}{2}\right)^2 + \varepsilon_d^2} \quad (5)$$

3. Elastoplastic two-stage solution for SSI in deep excavation

As discussed earlier, Franza and DeJong (2019) proposed a two-stage elastoplastic solution for SSI analysis of building response to tunneling induced ground movements. In this paper, the elastoplastic solution procedure is adapted to deep excavation scenarios and then incorporated into the computer program Analysis of Structural Response to Excavation (ASRE), originally developed by Franza and DeJong (2019).

3.1. Greenfield displacement

The first stage of the two-stage elastoplastic solution is to determine vertical and horizontal greenfield ground displacements ($\mathbf{u}^{cat}$ in Eq. (4)). The KJHH model (Kung et al., 2007) and the KSJH model (Schuster et al., 2009) are adopted in this paper because they consist of a complete estimation procedure that links horizontal wall deflection to vertical and lateral ground movement profiles. Moreover, the model uncertainty of the KJHH and KSJH are well documented, so the influence of their uncertainty on building damage is ready to be analyzed. However, the ground displacement profiles in both models are described discretely with 4 pivot points (A-D as shown in Fig. 2), and cannot be applied to the elastoplastic two-stage analysis directly, in which continuous ground displacement profiles are required. Therefore, a pair of shifted log-normal curves are fitted to the KJHH and KSJH ground displacement profiles in Fig. 2. The log-normal curves pass through pivot points A, B, and C in the KJHH and KSJH models exactly and smoothen the sharp corners. The fitted curves also coincide well with the displacements observed in case histories reported by (Kung et al., 2007) and (Schuster et al., 2009). The coefficient of determination (R^2) for the proposed vertical and lateral displacement profiles are 0.95 and 0.93 respectively, while the R^2 value for the original discrete KJHH and KSJH profiles are 0.92 and 0.88. Eq. (6) describes the formulation of the greenfield ground displacement profile proposed in this paper, where d is the distance from excavation, H_e is the depth of excavation, δ_{vm} and δ_{lm} are respectively the maximum vertical and lateral ground displacement.

$$\frac{\delta_v(d/H_e)}{\delta_{vm}} = \frac{1.14}{\frac{d}{H_e}+0.39}\frac{1}{0.46\sqrt{2\pi}}exp\left(-\frac{(\ln(d/H_e+0.39)-0.095)^2}{0.423}\right) \quad (6a)$$

$$\frac{\delta_l(d/H_e)}{\delta_{lm}} = \frac{2.14}{\frac{d}{H_e}+0.82}\frac{1}{0.44\sqrt{2\pi}}exp\left(-\frac{(\ln(d/H_e+0.82)-0.80)^2}{0.387}\right) \quad (6b)$$

3.2. Structural analysis models

Two types of structural analysis models are studied in this paper: an equivalent Timoshenko beam model and a 2-dimensional (2D) elastic frame model. Both models were implemented in ASRE by Franza et al. (2020a) and Franza and DeJong (2019). In the Timoshenko beam model, the target building is modeled as an equivalent isotropic Timonshenko beam defined by its dimensions, elastic modulus (E_b) and elastic over shear modulus ratio (E_b/G_b). The equivalent beam is discretized, and a stiffness matrix (**S**) is formulated and applied to Eq. (4). Burland et al. (1978) suggested that the value of E_b/G_b should be taken as 2.6 for isotropic walls and 12.5 for frame structures. The solution of ASRE consists of the displacement at each discretization node and the internal forces in each element. The Timoshenko beam model was evaluated with respect to field and centrifuge test results and provided reliable predictions for bearing wall structures on continuous foundations (Franza et al., 2020a).

The existing elastic 2D frame model considers each frame member as an isotropic elastic beam element and formulates the frame stiffness matrix with the displacement method. However, the previous elastic 2D frame model implementation is considered to be too simple because it only supports the modeling of structures with identical footings, one column on each footing, equal floor elevations, equal beam span widths and the same beam and columns dimensions. Moreover, infill walls, which can significantly affect the structure stiffness, were not previously considered. The structural analysis model for frame structures in ASRE is updated in this paper to include irregular frames and infill walls.

Fig. 3a schematizes the frame structure model developed in this paper. The beams and columns are discretized at each junction and each foundation element is discretized with a small element size. A fine grid is adopted for each foundation because the foundations are connected to soil-structure interface elements and the small element size more accurately captures the ground movements. Because all frame members deform elastically in this model and building self-weight loads are applied at beam and columns junctions, a coarse discretization of the frame is sufficient. In the updated frame structure model, footings with varying dimensions and footings connected to multiple columns can be modeled. The floor elevations and bay spans can be distinct at each frame panel, and each beam and column can have different dimensions and material properties. The stiffness of infill walls are modeled as equivalent diagonal compression struts. Eq. 7 is used to calculate the stiffness of the struts, as recommended by FEMA (1998), where t is the thickness of the infill panel, h and l are respectively the height and length of the infill panel, E_c and E_m denote the elastic moduli of column and infill respectively, θ is the inclination angle of the strut, I_c is the moment of inertia of the adjacent columns and H_w is the height of the infill wall, as shown in Fig. 3b. Diagonal compression struts are only placed when the diagonal strain is compressive. In other words, the tensile strength of the diagonal struts is assumed to be zero. The application of the proposed frame structure analysis model to a case study is demonstrated in a later section.

$$A_e = W_e t \quad (7a)$$

$$W_e = 0.175(\lambda h)^{-0.4}\sqrt{h^2+l^2} \quad (7b)$$

$$\lambda = 4\sqrt{\frac{E_m t sin(2\theta)}{4E_c I_c H_w}} \quad (7c)$$

3.3. Damage assessment

For Timoshenko beam models, the direct strain based approach by Franza et al. (2020b) is adopted in this paper because it overcomes possible errors due to the simplification in the calculation of $\frac{\Delta}{L}$ and β in the methods by Burland et al. (1978) and Son and Cording (2005) (See discussions in Appendix 1). In the direct strain based approach, the maximum internal forces N_m, M_m and V_m among all cross-sections of the beam are first computed with ASRE and $\varepsilon_{b(max)}$, $\varepsilon_{d(max)}$, and ε_h are calculated with Eq. (5) For a rectangular cross-section, κ and c are taken as $\kappa = \frac{10(1+\nu)}{12+11\nu}$ and $c = 3/2$, where ν is the Poisson's ratio of the beam. ε_{crit} is taken as the larger value of ε_b and ε_{dt}, and compared with the damage classification criterion by Boscardin and Cording (1989) (Table 1) to obtain a damage category of the building.

For the 2D elastic frame model proposed in this paper, damages to infill walls and the structural frame are evaluated separately. To evaluate the damage of infill walls, Son and Cording (2005)'s method is adopted. The vertical displacements (A_v, B_v, C_v, D_v) and lateral displacements (A_l, B_l, C_l, D_l) at the corners (A, B, C, D) of each infill panel are determined (See Fig. 4 for the geometry of a building unit). The slope, rigid body rotation (tilt), angular distortion (β) and lateral strain at top and bottom are calculated with Eq. (8). Afterwards, the critical strain of each infill wall can be estimated with Eq. (9) and (10), and the

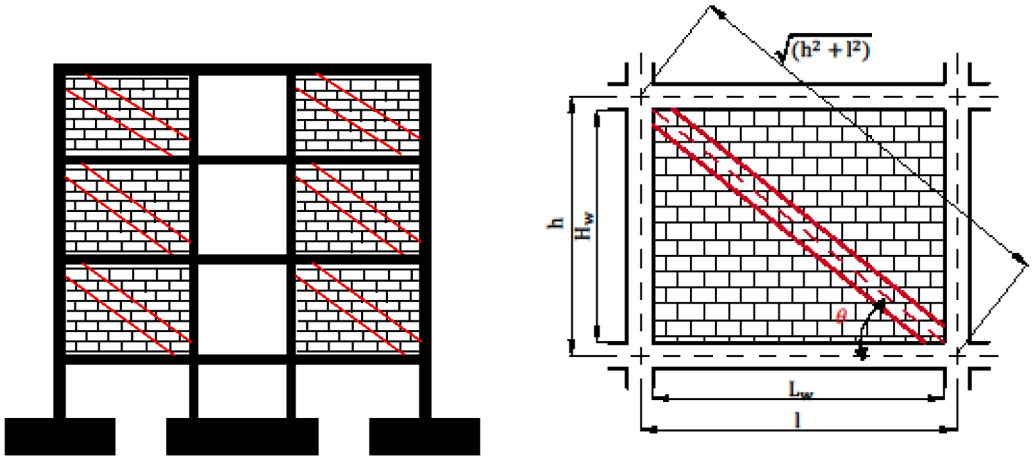

(a) Schematic frame model (b) Equivalent diagonal strut of masonry infill walls

Fig. 3. The proposed 2D elastic frame model.

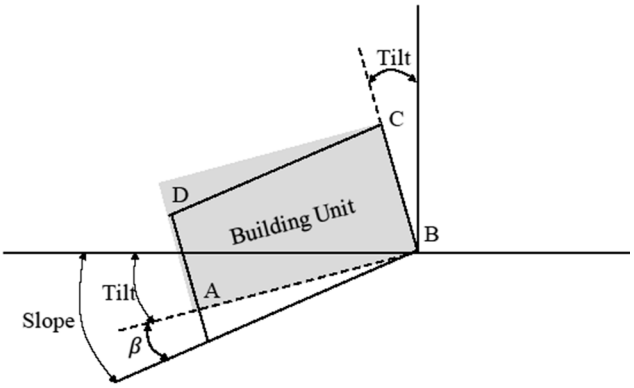

Fig. 4. Slope, tilt and angular distortion (β) of a building unit.

damage category of each infill wall is classified according to Son and Cording (2005)'s criterion in Table 1.

To evaluate the damage of the structural frame, the method of Ghobarah (2004) is adopted. Ghobarah (2004)'s method is originally used to evaluate building damage after an earthquake and inter-story drift ratio is considered as the engineering demand parameter to classify building damage. Ghobarah (2004) defined inter-story drift ratio by the difference of horizontal displacement of top and base floor divided by the floor elevation. In this definition, each floor is assumed to remain horizontal. However, in the case of excavation induced building deformation, each frame panel experiences both vertical and horizontal drifts (see Fig. 4). Therefore, the inter-story drift ratio is equivalent to the horizontal displacement difference after rotating the frame panel by the slope angle (i.e., drift ratio $= tan\beta$, where β is the angular distortion defined by Son and Cording (2005)). When β is small, it is assumed $tan\beta \approx \beta$. Therefore, assuming the drift-ratio is equivalent to angular distortion, the criterion of Ghobarah (2004) can be used to classify potential damage of each frame panel using Table. 2.

This proposed damage assessment method which considers both the structural frame and infill walls can provide an overall estimate of the building, but it also identifies locations of potential damage in the form of the ε_{crit} and β values that are calculated for each panel. The application of this method is demonstrated by a case study in a later section.

Table 2
Relationship between damage category and angular distortion (After Ghobarah (2004)).

State of damage	Ductile frame	Nonductile frame
No damage	0–0.2	0–0.1
Repairable damage		
a) Light (aesthetic) damage	0.2 – 0.4	0.1 – 0.2
b) Moderate (serviceability) damage	0.4–1.0	0.2–0.5
Irreparable damage (structural damage)	1.0 –1.8	0.5 –0.8
Severe damage (collapse)	1.8 –3.0	0.8 –1.0

$$
\begin{aligned}
Slope &= \frac{A_v - B_v}{L_w} \\
Tile &= \frac{(C_l - B_l) + (D_l - A_l)}{2H_w} \\
\beta &= Slope - Tile \\
\varepsilon_h(top) &= \frac{D_l - C_l}{L_w} \\
\varepsilon_h(bottom) &= \frac{A_l - B_l}{L_w}
\end{aligned}
\tag{8}
$$

$$
tan(2\theta_{max}) = \frac{\beta}{\varepsilon_h} \tag{9}
$$

$$
\varepsilon_{crit} = \varepsilon_h cos^2\theta_{max} + \beta sin\theta_{max} cos\theta_{max} \tag{10}
$$

4. Case studies

4.1. Singapore Art Museum

The first case study explored in this paper was originally published by Goh and Mair (2011). The east and west wings of the Singapore Art Museum (SAM), which were impacted by the construction of the Bras Basah subway station, are analyzed. The excavation was 35 m deep and is approximately 6 m away from the wings of the SAM. The excavation support system consists of a diaphragm wall and 5 layers of bracing. The soil beneath the SAM consists of four layers of clay with intermittent fluvial sand layers. The representative soil stiffness was reported to be 47 MPa. The structural behaviour of the SAM is dominated by four masonry walls with an average thickness of about 500 mm. The

settlement of four walls (SAM-1, SAM-2, SAM-4, SAM-5, see Fig. 5) and the non-suspended, tiled pavement (BBS-1, BBS-2, BBS-4, BBS-5) just outside the walls are monitored by precise levelling. The monitored settlement at BBS-1, 2, 4, 5 are considered as an approximation of corresponding greenfield ground settlement at SAM-1, 2, 4, 5. The height of the walls is around 9.7 m and the Young's modulus of the walls is reported to be 5GPa. The foundation is shallow and consists of soft timber layers. Consequently, the contribution of the foundation to the overall building stiffness is ignored. The stiffness of the structure is mostly due to the masonry walls as the floor slabs are thin and much more flexible in comparison, as suggested by Goh and Mair (2011).

Since the structure section perpendicular to the deep excavation consists of continuous walls, the Timoshenko beam model is used to analyze the walls. SAM-1 and SAM-5 are modeled as beams with lengths of 28 m, and SAM-2 and SAM-4 are modeled as beams with lengths of 15 m. All four beams are 9.5 m high and 0.5 m thick. Since the building material is identical for these building sections, a constant elastic modulus of 5GPa, as suggested by Goh and Mair (2011), is adopted. A value of 6 is taken for $\frac{E_b}{G_b}$ to account for the openings in the walls. The maximum horizontal deflection (δ_{hm}) of the diaphragm wall, vertical deformation ratio (R_v), lateral deformation ratio (R_l) are first calculated according to the KJHH and KSJH models. Vertical and lateral ground movement profiles are then estimated with Eq. (6). In other words, these were prediction values and prediction ground settlement curves, assuming no knowledge of the actual settlement. Fig. 6a shows the analysis and monitoring results for SAM-1 and SAM-5. Fig. 6b shows the analysis and monitoring results for SAM-2 and SAM-4. The support system and underground conditions are assumed to be equal for the four walls which results in identical ground movement profiles for the four analyzed sections (Fig. 6). Note that since walls SAM-1 and SAM-5 are identical, the analysis results are also identical. The analysis results for SAM-2 and SAM-4 are also identical for the same reason.

It is observed that the measured ground displacement of BBS-1 and BBS-5 are significantly different, despite that these two scenarios are identical from a prediction perspective. This indicates that a single deterministic ground settlement profile prediction, using the KJHH model or otherwise, will not be able to predict both of the scenarios. The same observation holds for BBS-2 and BBS-4. Goh and Mair (2011) explained the difference in the monitoring results by a different order of the construction activities at the east wing and west wing of SAM. This

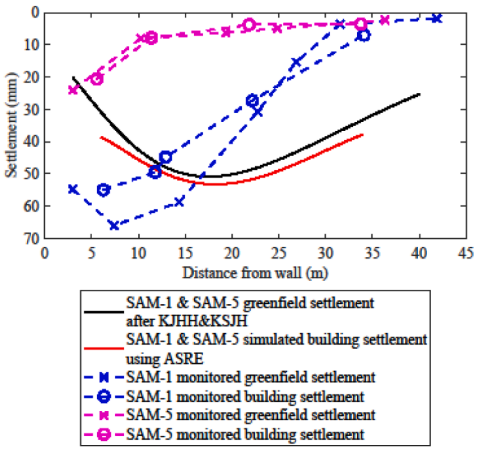

(a) SAM-1 & SAM-5

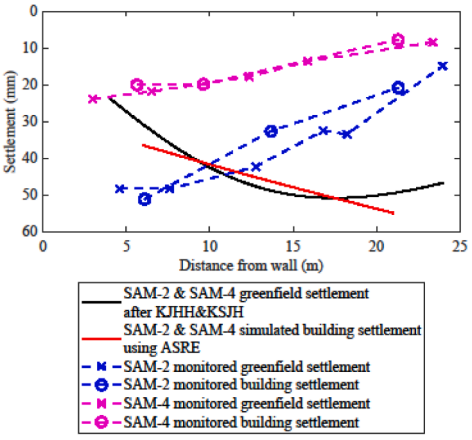

(b) SAM-2 & SAM-4

Fig. 6. Singapore Art Museum case study. Predicted greenfield settlement profiles using the KJHH & KSJH models, predicted building settlement profiles using ASRE, and monitored settlement profiles.

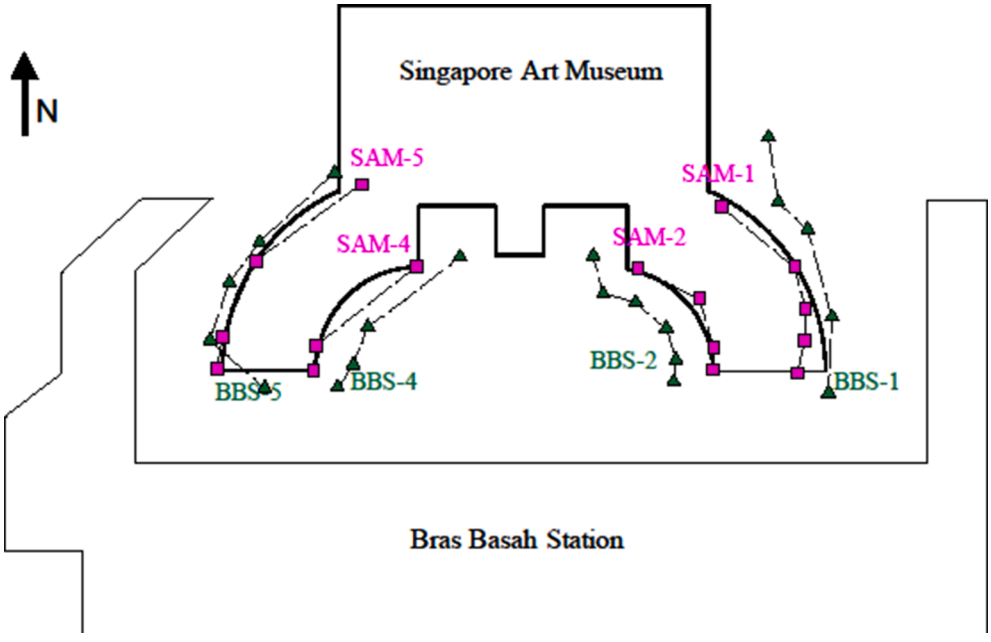

Fig. 5. Plan view showing the locations of building settlement (in squares) and ground settlement (in triangles) monitoring points (after Goh and Mair (2011)).

discrepancy between monitored ground displacements implies that notable uncertainty exists in the prediction of ground movements. Moreover, Goh and Mair (2011) reported that SAM-5 behaved in a more flexible manner compared to SAM-1 even though their structures are similar. This might be explained by some existing structural damage in SAM-5 and it implies that modeling of existing buildings, especially historical buildings, could be associated with large uncertainty. In summary, the uncertainty observed in this case study exists in the estimation of δ_{vm}, width of the settlement profile and building stiffness. Because horizontal ground displacement was not monitored, the accuracy or uncertainty associated with the KSJH model can not be evaluated.

A back-analysis was then undertaken to study the uncertainty in the above modeling method. In the back-analysis δ_{vm} is taken as the interpolated maximum value of the measured settlement profile. The width of the settlement profile is adjusted by introducing a scaling term (η) to Eq. (6), as shown in Eq. (11). The value of η for each wall is determined by minimizing the mean squared error $\frac{1}{n}\sum_i^n(\delta_v(x)-\widehat{\delta}_v(x))^2$, where n is the number of monitoring points, $\delta_v(x)$ are the monitored displacements and $\widehat{\delta}_v(x)$ are the values predicted by Eq. (11). The elastic stiffness of SAM-5 was reduced to 1 GPa by a trial and error method to recover the monitored building settlements. The back-analysis results are shown in Fig. 7. The analysis results for SAM-1, SAM-2 and SAM-4 imply that if the ground settlement profile is estimated accurately, the two-stage elastoplastic solution can predict building response reasonably well, even with a nominal value of structural stiffness. However, the analysis results of SAM-5 indicate that the uncertainty in the modeling of the structure (i.e., the reduction in building stiffness due to potential existing damage) should also be considered in the analysis of excavation induced structural damage. The uncertainty in the whole analysis framework is studied comprehensively in section 5.

$$\begin{aligned}\delta_v(x) &= \delta_{vm}\frac{1.14}{\frac{x}{\eta}+0.39}\frac{1}{0.46\sqrt{2\pi}}exp\left(-\frac{\left(\ln\left(\frac{x}{\eta}+0.39\right)-0.095\right)^2}{0.423}\right)\\ \delta_l(x) &= \delta_{lm}\frac{2.14}{\frac{x}{\eta}+0.82}\frac{1}{0.44\sqrt{2\pi}}exp\left(-\frac{\left(\ln\left(\frac{x}{\eta}+0.82\right)-0.80\right)^2}{0.387}\right)\end{aligned} \tag{11}$$

4.2. Chicago Frances Xavier Warde School

The second case study explored in this paper was originally published by Finno and Bryson (2002) and Finno et al. (2005). The analyzed structure is a cross-section of Chicago Frances Xavier Warde School (ChiFXWS), which was impacted by the construction of the subway renovation project on State Street and Chicago Avenue. The cross-section, as shown in Fig. 8, is a three-story concrete frame structure

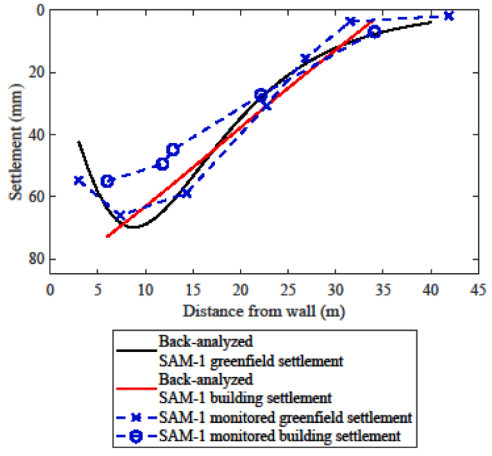

(a) Back-analyzed and monitored settlement of SAM-1

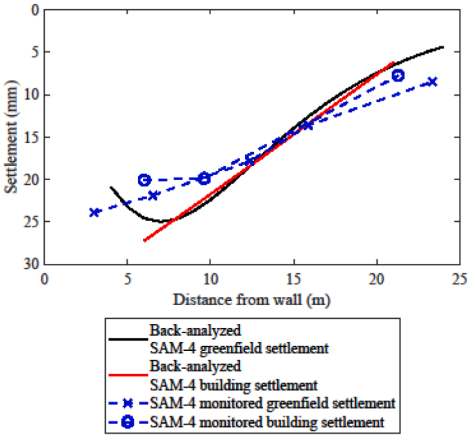

(c) Back-analyzed and monitored settlement of SAM-4

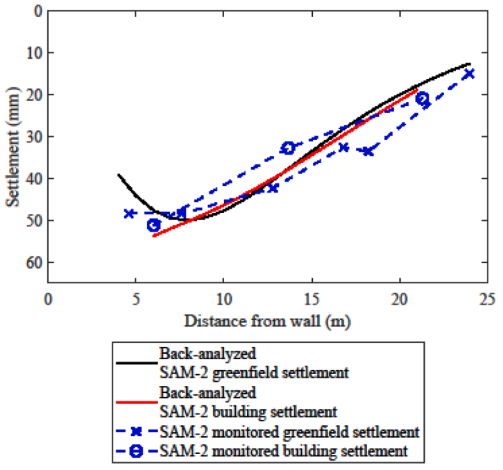

(b) Back-analyzed and monitored settlement of SAM-2

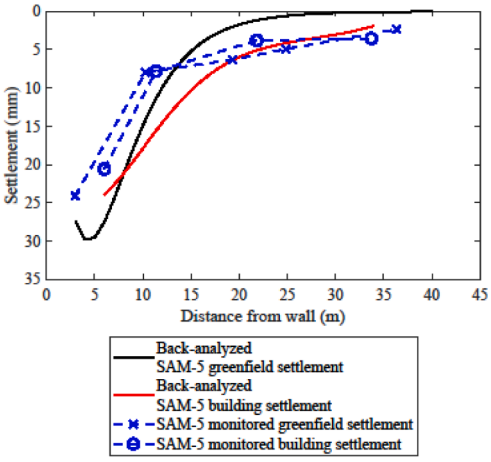

(d) Back-analyzed and monitored settlement of SAM-5

Fig. 7. Settlement of SAM after applying back-analyzed δ_{vm} and..δ_{hm}

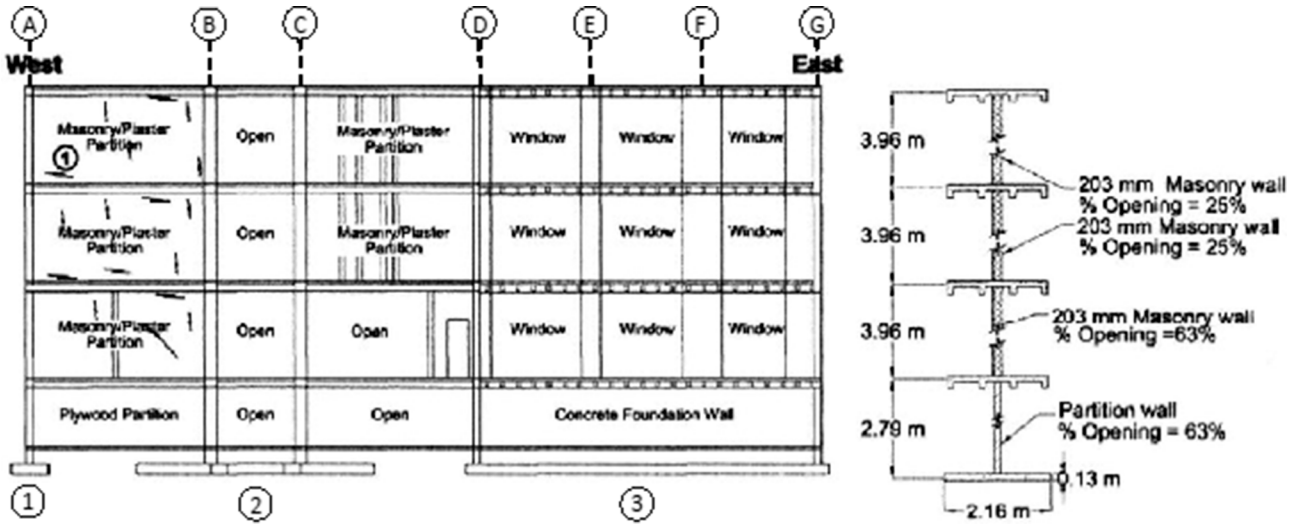

Fig. 8. Elevation view of the analyzed cross-section of Chicago Frances Xavier Warde School (ChiFXWS) (after Finno et al. (2005)).

with brick partition walls and a basement. The floor system at each level consists of a reinforced concrete pan-joist and is supported by interior concrete columns and beams, and masonry bearing walls around the perimeter. The interior columns and perimeter walls rest on three separated footings. The excavation is 1.2 m to the west of the frame and is almost perpendicular to the frame. The excavation depth is 12.2 m and the excavated soil is soft to medium clay. The excavation support system consists of a secant pile wall with three levels of supports. The building settlement is monitored at 5 points along the cross-section at basement level or 1 m above grade with optical survey points. The cross-section is modelled with the 2D elastic frame proposed in this paper. The partition walls are modeled as diagonal compression struts with Eq. 7, where the elastic modulus of masonry is taken as 12.5GPa and the elastic modulus of concrete elements are taken as 36GPa. The concrete foundation wall at the east part of the frame is also modeled using diagonal compression struts but the value of E_m is taken as 36 GPa. Because the exact values of the material properties are not reported by Finno and Bryson (2002) and Finno et al. (2005), typical values are adopted. The analysis of this structure here is not aimed to recover the response of the structure exactly, but to simulate the typical situation in design practice, in which the material properties are unknown, and to demonstrate the uncertainty associated with current design procedures.

The settlement of this 2D elastic frame is calculated with the two-stage elastoplastic methods and ASRE. The greenfield input to the two-stage analysis is first estimated with the KJHH and KSJH models. The estimated value of δ_{vm} and δ_{lm} are 25 mm and 20.9 mm respectively, and a ground movement profile is determined with Eq. (6). The monitored building settlement and computed building settlement are plotted in Fig. 9a. It is observed that the settlement determined from the two-stage analysis is close to the monitored values for footing 2 and footing 3, while the analyzed settlement of footing 1 is approximately one half of the monitored value. Because there is not any concentrated load applied at footing 1, it is not reasonable to observe a building settlement 4 times larger than the greenfield settlement. Therefore, it can be argued that the predicted greenfield settlement profile is not accurate and this uncertainty is an important reason for the discrepancy between predicted and monitored building settlement. A back-analysis is then conducted by adjusting the greenfield settlement with Eq. (11). The back-analysis result is shown in Fig. 9b. The purpose of the back-analysis is to show that when the uncertainty of δ_{vm} and trough width is taken into account, the monitored building settlement can be recovered in one realization of the probabilistic analysis framework, as will be discussed later.

After the building displacement is computed, the damage level of the

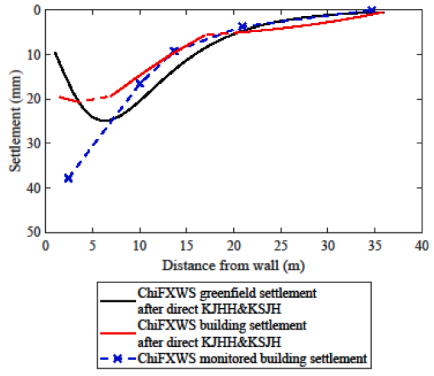

(a) Analyzed and monitored settlement of ChiFXWS after direct KJHH & KSJH

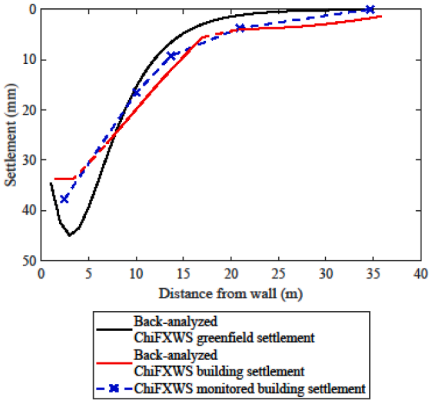

(b) Back-analyzed and monitored settlement of ChiFXWS

Fig. 9. Chicago Frances Xavier ward School case study. Predicted greenfield settlement profiles using the KJHH & KSJH models, predicted building settlement profiles using ASRE, and monitored settlement profiles.

frame is analyzed with the method proposed for the 2D elastic frame model. In the prediction analysis, i.e., the direct application of the KJHH and KSJH models to obtain the predicted greenfield settlement, the frame panels between span C-D (see Fig. 8) experienced slight to moderate levels of damage at the first floor and the frame panels between span B-C experienced negligible to slight damage at each floor. The

angular distortion of the panels between span C-D is around 0.26% and the angular distortion between span B-C increased from 0.10% on the first floor to 0.11% on the third floor. The maximum partition wall strain is 0.13%, which occurs at the partition walls between span C-D at the second and the third floor. The strain levels in other partition walls are small and negligible. The distribution of damage coincides with the cracks observed after the construction works. Finno and Bryson (2002) reported that damage mainly occurred at the west part of the building and cracks were observed at the infill walls at the second and third floor. The back-analysis results suggest a similar distribution of damage with slightly larger strain in each frame panel and infill wall.

5. Uncertainty analysis

In the case studies, it is observed that the model uncertainty of KJHH & KSJH influences building responses significantly. Additionally, the analysis of surface structures also experiences uncertainty caused by incompleteness of knowledge (e.g., unavailable material properties) and model uncertainty (e.g., simplification of a structure as an equivalent beam or a 2D elastic frame). These uncertainties associated with greenfield displacement estimation and surface structure analysis are called input uncertainty of the second stage assessment. The input uncertainty can be reduced with further analysis such as detailed modeling of the excavation system or a comprehensive survey of the building. However, it is typically not feasible to reduce all of the input uncertainty mentioned above during a simplified second stage assessment. Therefore, it is important to study which input causes the most uncertainty in the output of the second stage assessment, so that more reliable damage prediction can be achieved with the least amount of effort on reducing the input uncertainty. This section uses a variance based sensitivity analysis (Sobol's method) to study what is the major source of uncertainty in the second stage assessment and how to reduce the uncertainty of the predicted building damage efficiently.

5.1. Uncertainty sources

In order to study the influence of uncertainty sources on building damage predictions, the input uncertainty needs to be quantified. A common method to quantify an uncertain parameter is to model the parameter as a random variable with a certain probabilistic density distribution. In this section, uncertainty sources of the two case studies are identified and quantified.

As shown by the previous analyses of the SAM and ChiFXWS case studies, the model uncertainty of the KJHH & KSJH models may have significantly influenced the predicted building damage. In the KJHH & KSJH models, ground settlement profiles are described based on four parameters: the maximum wall deflection (δ_{hm}), vertical deformation ratio (R_v), lateral deformation ratio (R_l) and trough width parameter (η). The uncertainty of δ_{hm}, R_v and R_l are quantified by Kung et al. (2007) and Schuster et al. (2009) as Eq. (12), where $\overline{\delta}_{hm}$, $\overline{R}_v$ and $\overline{R}_l$ are the mean values of δ_{hm}, R_v and R_l, and can be estimated by adopting the regression equations in the KJHH & KSJH models. The uncertainty of δ_{hm}, R_v and R_l are described with corresponding bias factors (BF_{hm}, BF_v and BF_l), which are statistically independent random variables. Consequently, δ_{hm}, R_v and R_l are also random variables because they are a product of random variables and constants. It is important to notice that δ_{hm}, R_v and R_l are highly correlated, but they are conditional independent to each other when they are conditioned on the input parameters of the regression equations in the KJHH & KSJH models. In other words, when the underground conditions and excavation system are defined, the model errors in the estimation of δ_{hm}, R_v and R_l are statistically independent to each other. The mean and standard deviations for BF_{hm}, BF_v and BF_l are reported by Kung et al. (2007) and Schuster et al. (2009), as shown in Table. 3. BF_{hm}, BF_v and BF_l are modelled as normally distributed, which is a common practice in statistical studies of geotechnical engineering (Baecher and Christian, 2005).

Table 3
Quantification of input uncertainty in the analysis of SAM and ChiXFWS.

Random Variable	Statistical model
BF of Maximum wall deflection (BF_{hm})	Normal(1, 0.25^2)
BF of Vertical deformation ratio (BF_v)	Normal(1, 0.13^2)
BF of Lateral deformation ratio (BF_l)	Normal(1, 0.11^2)
Ground displacement profile width parameter (η)	Normal(1, 0.16^2)
Elastic modulus of equivalent beam model (E_b (GPa))	Lognormal(1.57, 0.086)
Elastic over shear modulus ratio of equivalent beam model (E_b/G_b)	Lognormal(1.54, 0.15)
Concrete compressive strength (f'_c (MPa))	Uniform(20, 40)
Masonry elastic modulus (E_m (GPa))	Uniform(6, 21)
2D frame beam width (b_b (m))	Normal(5.76, 0.58^2)

Kung et al. (2007) and Schuster et al. (2009) also indicated that uncertainty exists in the estimation of the shape of ground displacement profiles. By observing the case histories used to derive Eq. (2) and (3), it is concluded that the pivot point A does not vary among the case histories while the distances of point B, C and D to the excavation wall show large fluctuations. To quantify the uncertainty of the ground displacement profile shape, a scale factor η is added to Eq. (6) to shrink or elongate the ground displacement profile width (see. Eq. (11)). In the case histories reported by Kung et al. (2007) and Schuster et al. (2009), the distance of pivot point B to the excavation wall varies in the range $0.3H_e$ to $0.7H_e$ and $0.6H_e$ to $1.4H_e$ for vertical displacement and lateral displacement respectively. These variance ranges correspond to a η with a range from 0.6 to 1.4. Because the locations of the pivot points are mean values from a regression analysis and η is their relative error, it is reasonable to assume η follows a normal distribution centered at 1. The standard deviation of η is estimated as 0.16 to ensure a 99% likelihood that η is in the interval $(0.6, 1.4)$.

For the equivalent Timoshenko beam model used to analyze the SAM, uncertainty exists in the estimation of the equivalent elastic modulus (E_b) and elastic over shear modulus ratio (E_b/G_b). As suggested by Dimmock and Mair (2008 E_b can be taken according to the building material and E_b/G_b can be taken as 2.6 for bearing wall structures with no openings. However, these values are roughly estimated with ignorance of the natural material variability, existing damage and structure details such as openings and different building lay-outs. Son and Cording (2007) concluded that the value of E_b/G_b has a larger variance range and is harder to estimate compared to E_b. In this study, the coefficient of variance (c.o.v.) of E_b for SAM is selected to be 30% and the c.o.v of E_b/G_b for SAM is selected to be 45%. These c.o.v. are selected by trial and error so that the 99% coverage intervals of E_b and E_b/G_b are reasonable according to the information provided by Goh and Mair (2011). The mean value for E_b and E_b/G_b are taken as 5 GPa and 6 respectively, which are the same as the values adopted in the deterministic study previously. The type of probability distribution for E_b and E_b/G_b are modeled as log-normal distribution, as commonly adopted for positive definite random variables (Ayyub and Klir, 2006). The 99% probability coverage intervals of E_b and E_b/G_b are $(3.84, 5.98)$ and $(3.40, 8.80)$.

For the elastic 2D frame model used to analyze ChiFXWS, the uncertainty mainly comes from the estimation of the stiffness of columns, beams and infill walls. This is because the reinforcement layout of columns and beams are not available and the material properties are roughly estimated. The compression strength of concrete (f'_c) is estimated as 30 MPa and the corresponding elastic modulus is $E_c = 4700\sqrt{f'_c} = 26GPa$, as suggested by ACI 318 (2008). The elastic modulus for beams and columns are amplified to 36 GPa based on an assumption of 5% reinforcement ratio. In reality, the compressive strength of normal strength concrete is in the range of 20 MPa to 40 MPa, and no information is available to narrow this range for the case of ChiFXWS. Therefore, f'_c is modeled as a random variable uniformly distributed between 20 MPa and 40 MPa. Consequently, the elastic

modulus of concrete is a random variable depending on f'_c. According to the Brick Industry Association (1992), the elastic modulus of brick masonry assemblage (E_m) is roughly proportional to its compression strength, and has a variance range of 6 GPa to 21 GPa. Similar to f'_c, there is no information with respect to the compressive strength of masonry used in ChiFXWS. Therefore, the masonry compressive strength is also assumed to follow a uniform distribution. Because E_m is linearly dependent on the masonry compressive strength, it can be assumed that E_m is also uniformly distributed (i.e., $E_m \sim Uniform(6,21)$). Such uninformative uniform distribution with bounds based on data or expert knowledge is usually selected when there is inadequate knowledge in the most likely values of the variables (e.g., Baecher and Christian (2005) and Edeling et al. (2021)).

Another input uncertainty considered in the analysis of ChiFXWS is the width of floor slab flanges. In the previous deterministic analysis, the flange width of floor slabs included in the analysis is taken as 8 times the slab thickness as recommended by ACI 318 (2008). Therefore, an equivalent rectangular beam with 5.76 m width and 0.06 m depth is adopted. The equivalent rectangular beam has the same axial stiffness and bending stiffness as the sum of the beam and floor flanges. However, the stiffness of transverse beams is ignored in the deterministic analysis. To account for the effect of the transverse elements on the stiffness of the 2D frame model, the beam width (b_b) is modeled as a normal random variable with a mean of 5.76 m and a c.o.v. of 10%. The 99% probability coverage of b_b is $(4.28, 7.24)$. All the uncertainties studied in this paper are summarized in Table. 3.

$$\begin{aligned} \delta_{hm} &= BF_{hm}\bar{\delta}_{hm} \\ R_v &= BF_v\bar{R}_v \\ R_l &= BF_l\bar{R}_l \end{aligned} \tag{12}$$

5.2. Sensitivity analysis

After the input uncertainty is quantified, Sobol's (variance based) sensitivity analysis is deployed to study the effect of each uncertainty input on building damage prediction. Sobol's sensitivity analysis is one of the most robust global sensitivity analysis methods (Saltelli et al. (2008, 2010)) to decompose and attribute the variance of a system to each input variable. The contribution of each input variable is quantified with its Sobol's indices, and the first order indices (S_i) and the total effect indices ($S_{T,i}$) are the most commonly adopted sensitivity measures. The definition of S_i and $S_{T,i}$ can be found in Saltelli et al. (2008) and Appendix 2. The first order effect index measures the variance of system output (Y) when only the i_{th} input random parameter (X_i) varies but averaged over the variation of all the other input parameters. The total effect index measures X_i's contribution to the output variance after interacting with all the other input parameters. Larger Sobol's indices imply that the corresponding input parameter is more responsible for the uncertainty of the system output, and reducing the variance associated with such input will lead to more reduction in the variance of system output. S_i and $S_{T,i}$ are computed with the quasi-Monte Carlo method, and the procedures can be found in Appendix 2.

In the analysis of the SAM, the parameter used to classify building damage (the engineering demand parameter) is the critical strain ε_{crit}. Therefore, ε_{crit} is selected as the output Y in the sensitivity analysis and the Sobol's indices of BF_{hm}, BF_l, BF_v, η, E_b and E_b/G_b with respect to ε_{crit} are computed. In the analysis of ChiFSWS, the maximum frame panel distortion (β_{crit}) and maximum infill wall strain $\varepsilon_{crit(infill)}$ are used as engineering demand parameters, and their Sobol's indices are computed. The sensitivity analysis is done in two stages. In the first stage, only uncertainty of ground movements (i.e., BF_{hm}, BF_l, BF_v and η) are considered. This stage aims to study which part of the KJHH & KSJH models induced the most uncertainty in damage prediction. In the second stage, all the parameters in Table 3 are considered. The purpose of the second stage is to study whether the ground movement or the structure models are more responsible for the uncertainty of the building damage assessment.

The left column of Fig. 10 shows the results of the first stage sensitivity analysis. It is observed that among δ_{hm}, R_v, R_l and η, δ_{hm} caused most uncertainty in the estimation of ε_{crit}, $\varepsilon_{crit(infill)}$ and β. For the case of SAM-1 and SAM-5, almost all the uncertainty comes from the uncertainty associated with δ_{hm}, while for SAM-2 and SAM-4, the trough width parameter η also contributes a considerable amount of uncertainty. This may imply that an accurate estimation of η may reduce the uncertainty in damage prediction of structures with short spans, while the uncertainty of long span structures has a weaker correlation with η. In the analysis of ChiFXWS, Sobol's indices computed based on β_{crit} and $\varepsilon_{crit(infill)}$ are almost the same. This suggests that the value of β_{crit} and $\varepsilon_{crit(infill)}$ are highly related to each other. About 80% of the uncertainty in the estimation of β_{crit} and $\varepsilon_{crit(infill)}$ comes from δ_{hm} and 20% of the uncertainty comes from R_v. The uncertainty of R_l and η have nearly zero effect on the prediction of damage in ChiFXWS.

The right column of Fig. 10 shows the results of the second stage sensitivity analysis. It is observed that the indices of ground settlement input decreased because the uncertainty from the structure models is also included. In the analysis of SAM-1 and SAM-5, the total amount of uncertainty caused by E_b and E_b/G_b are almost identical to the uncertainty caused by the ground settlement model. In the analysis of SAM-2 and SAM-4, E_b/G_b showed a stronger contribution compared to the analysis of SAM-1 and SAM-5. This implies that shorter span structures are more sensitive to the uncertainty in the equivalent Timoshenko beam model, and both E_b and E_b/G_b are important sources of uncertainty in this circumstance. Future studies and field investigations to more accurately qualified E_b and E_b/G_b could be valuable to reduce the uncertainty in building damage assessments. In the analysis of ChiFXWS, it is observed that the uncertainty of f_c and b_b caused almost zero uncertainty in the prediction of both β_{crit} and $\varepsilon_{crit(infill)}$. In contrast, the uncertainty of infill wall stiffness (represented by E_m) show an effect on β_{crit} and $\varepsilon_{crit(infill)}$, which implies that proper modeling of infill walls may be important to achieve accurate damage predictions. However, the Sobol's indices which correspond to E_m are about 1/7 of the indices corresponding to δ_{hm}. Therefore, a better estimation of δ_{hm} is the most efficient way to reduce the uncertainty in this system. Comparing the analysis of the Timoshenko beam model and the 2D elastic frame model, it is observed that the Timoshenko beam model introduces more uncertainty in building damage predictions because there are more simplifications when the whole structure is modeled as an equivalent beam. The 2D elastic frame model is more complex and consists of more input parameters. Since many input parameters of the 2D elastic frame model can be evaluated accurately (e.g. floor elevation, beam span and column dimensions), they are considered with zero uncertainty and treated as constants in the analysis. Therefore, the uncertainty of the structural analysis model in a system using a 2D elastic frame model is less critical, and a better estimation of the ground settlement will reduce the uncertainty of building damage prediction more significantly.

6. A probabilistic analysis approach

The analysis in previous sections demonstrated the uncertainty in the early stage building damage assessment. One way to reduce the uncertainty is to reduce the input uncertainty, for example, using finite element analysis to estimate ground displacement rather than KJHH & KSJH. Such advanced models require more effort in the analysis and are usually unfeasible in the early stage assessment. Another method to deal with the uncertainty is to carry the uncertainty in the analysis framework and propagate the uncertainty from input parameters to engineering demand parameters (e.g., ε_{crit}). In this paper, this method is called probabilistic analysis approach and the result of this analysis approach is the empirical probability density distribution of the engineering demand parameters for the target building. The empirical probability density distribution will provide a level of confidence when

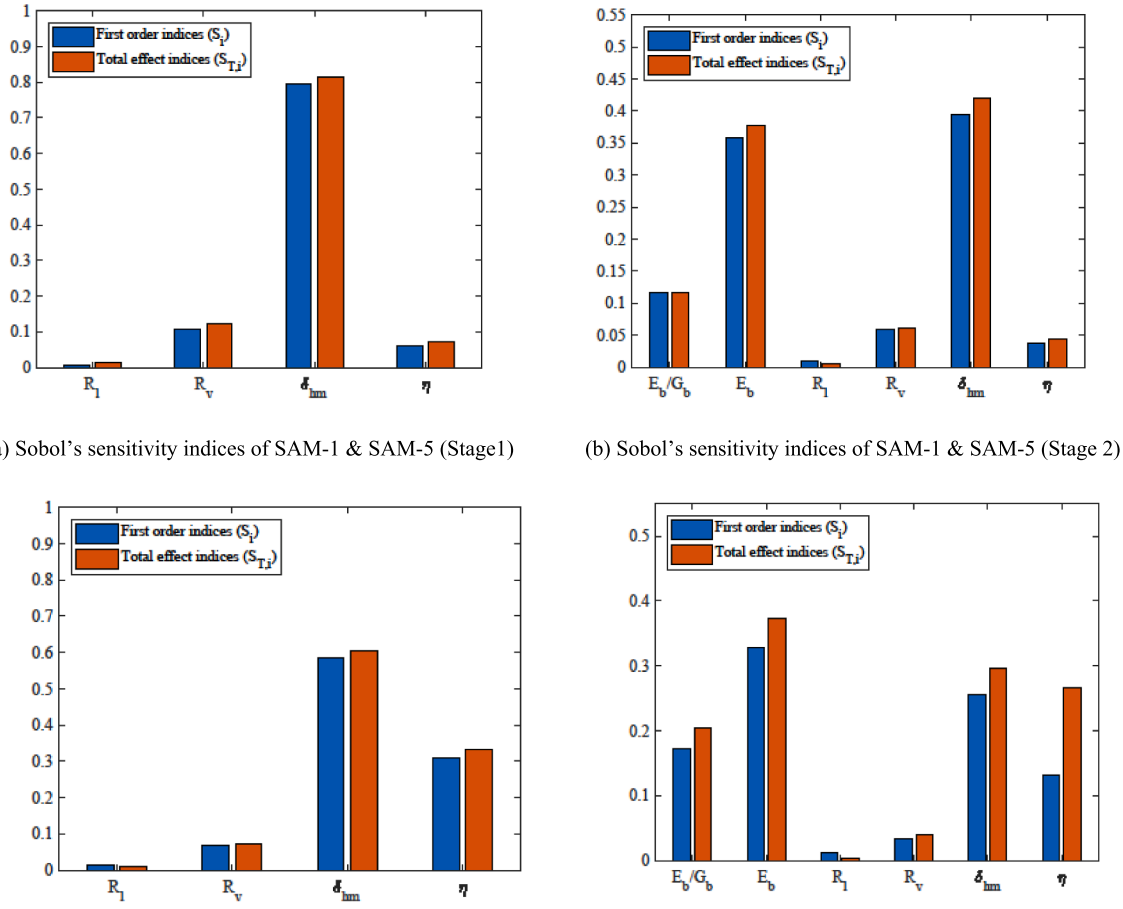

(a) Sobol's sensitivity indices of SAM-1 & SAM-5 (Stage1)

(b) Sobol's sensitivity indices of SAM-1 & SAM-5 (Stage 2)

(c) Sobol's sensitivity indices of SAM-2 & SAM-4 (Stage 1)

(d) Sobol's sensitivity indices of SAM-2 & SAM-4 (Stage 2)

Fig. 10. Sobol's indices for SAM and ChiFXWS.

the damage in a structure is classified. A comparison of the deterministic and probabilistic analysis approach of excavation induced adjacent building damage classification is shown in Fig. 11.

In the proposed probabilistic analysis approach, the uncertainty of the estimated ground settlement and structural analysis models are first quantified, and this step is called uncertainty input quantification. The quantification process described previously in sensitivity analysis is an example of uncertainty input quantification for SAM and ChiFXWS. In each project, the input uncertainty quantification will be unique, and should be done by experts based on whatever local site information is available. The quantified uncertainty input describes how much confidence the practitioners have with their model or their assumptions and this step is crucial to obtain a meaningful output from the probabilistic analysis approach.

After quantifying the uncertainty input, the uncertainty is propagated from input parameters to engineering demand parameters (EDP) with Monte-Carlo simulation and a soil-structure-interaction program, such as ASRE. Because the soil-structure-interaction process is highly nonlinear, the Monte-Carlo simulation method is one of the most robust methods to estimate the probabilistic characteristics of the EDPs. There are also other methods to estimate the probabilistic behavior of output of nonlinear systems, for example, local and global reliability analysis. In local reliability analysis, the response surface of the nonlinear system is estimated with first-order (FORM) or second-order (SORM) functions, while in global reliability analysis, the response surface is usually approximated as a Gaussian process model. Both local and global reliability introduces bias in the analysis because of the approximation made for the response surface. However, according to the law of large numbers, Monte-Carlo simulation converges to unbiased results when the number of simulations is sufficiently large. The drawback of the Monte-Carlo method is that a large number of model evaluations (usually more than thousands of evaluations) is required to reach convergence, which is unfeasible in analysis with large numerical models. Surrogate model methods, which approximate the system response surface with different types of fast numerical models (e.g., neural networks and support vector machine), is a common method used in Monte-Carlo simulations of large numerical models. However, surrogate modelling is not used in the proposed framework because: 1) at the early assessment stage of excavation works, full scale models are generally not available; 2) even if a full scale model is available, creating a reliable surrogate model requires a sufficient amount of evaluations of the model, which again causes large computational cost.

Because common reliability analysis may introduce bias and surrogate models are not available in the second assessment stage of potential building damage, a Monte-Carlo simulation with the direct soil-structure-interaction model through ASRE is adopted in the proposed analysis approach. To ensure an affordable computation time, the computer program ASRE was optimized with a parallel computation strategy and high-performance linear solvers. The computation time per 1000 simulations was reduced from around 3000 s to 150 s for the analysis of SAM-1 and around 8000 s to 500 s for the analysis of ChiFXWS. The optimized ASRE was then integrated into a computer program called Uncertainty Quantification in Excavation Structure Interaction (UQESI), in which uncertainty propagation and sensitivity

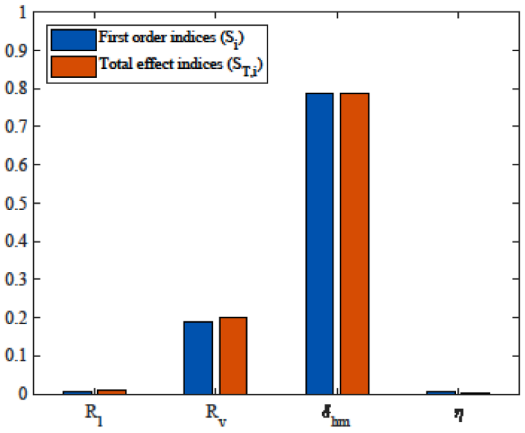

(e) Sobol's sensitivity indices for β_{crit} of ChiFXWS (Stage 1)

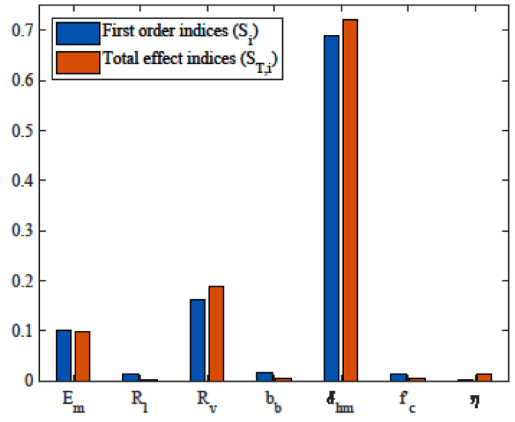

(f) Sobol's sensitivity indices for β_{crit} of ChiFXWS (Stage 2)

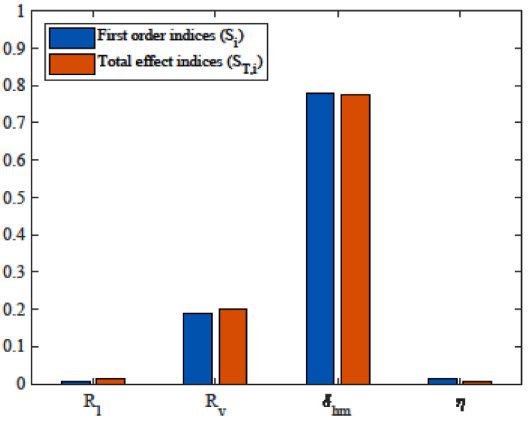

(g) Sobol's sensitivity indices for $\varepsilon_{crit(infill)}$ of ChiFXWS (Stage 1)

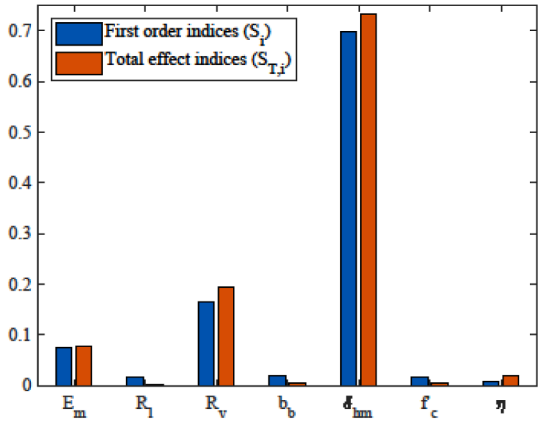

(h) Sobol's sensitivity indices for $\varepsilon_{crit(infill)}$ of ChiFXWS (Stage 2)

Fig. 10. (*continued*).

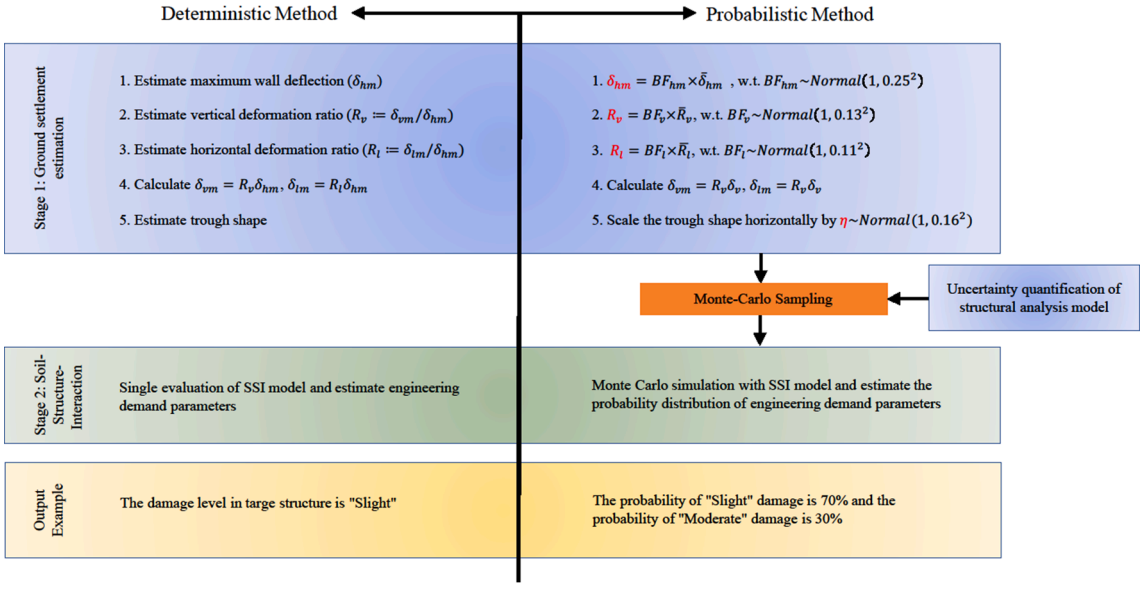

Fig. 11. Deterministic and probabilistic analysis approaches.

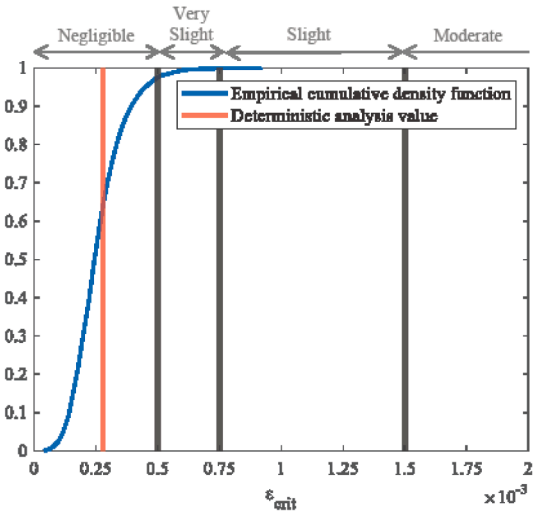

(a) Probabilistic assessment results of ε_{crit} in SAM-1 and SAM-5

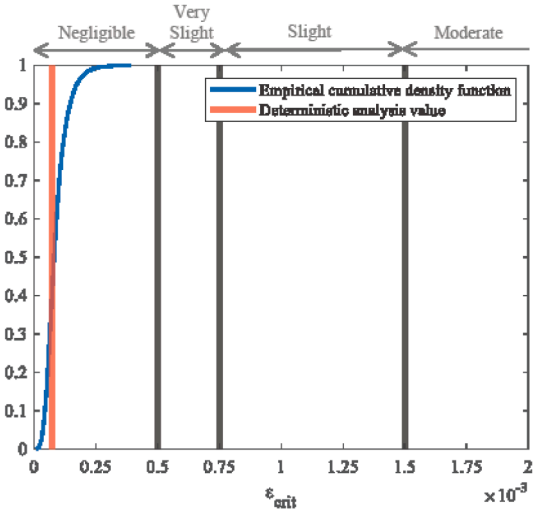

(b) Probabilistic assessment results of ε_{crit} in SAM-2 and SAM-4

Fig. 12. Probabilistic analysis results of SAM.

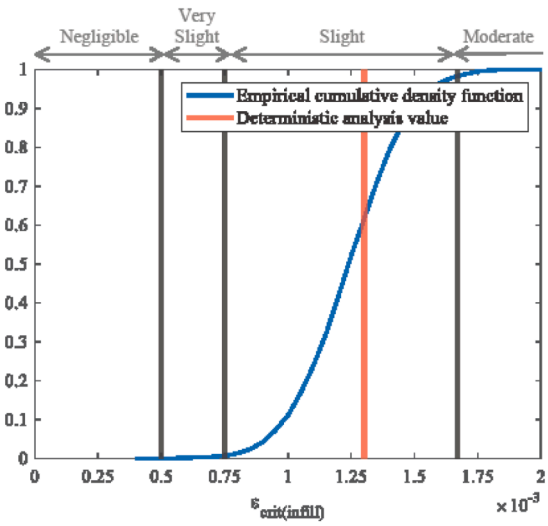

(a) Probabilistic assessment results of $\varepsilon_{crit(infill)}$ in ChiFXWS

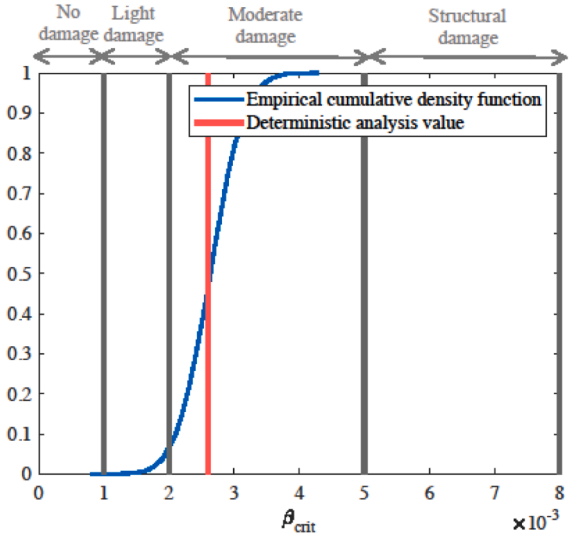

(b) Probabilistic assessment results of β_{crit} in ChiFXWS

Fig. 13. Probabilistic analysis results of ChiFXWS.

analysis are done. UQESI can also be used for uncertainty quantification and sensitivity analysis when other SSI models or surrogate models are adopted in the proposed probabilistic approach.

Figs. 12 and 13 shows the analysis results of SAM and ChiFXWS with the proposed probabilistic analysis approach, using the uncertainty inputs previously used in the sensitivity analysis (Table. 3). For SAM-1 and SAM-5, there is about 30% probability that the deterministic analysis results underestimate the potential damage. The probability of underestimating damage for SAM-2 and SAM-4 is about 50%. In the analysis of ChiFXWS, the probability of underestimating potential damage quantified by $\varepsilon_{crit(infill)}$ and β are 40% and 53% respectively. As expected, the deterministic analysis results do not provide an upper bound of potential damage. For SAM-1/5, SAM-2/4 and ChiFXWS, the damage categories predicted based on the probabilistic and deterministic analysis results are the same (i.e., there is approximately 100% probability that the structure will experience the damage category predicted with the deterministic analysis). This provides great confidence in the predicted damage category despite the large uncertainty in ground settlement estimation and structural modeling of SAM and ChiFXWS. In our view, this level of confidence is of great benefit, because it demonstrates that no further field investigation or model refinement is needed to be confident in the level of damage predicted. In contrast, a previous study (Zhao et al., 2021) on tunneling-induced settlement damage demonstrated that in other scenarios, the range of predicted damage can be much larger, and can span several damage category thresholds. This contrast demonstrates the benefit of quantifying the uncertainty. Specifically, deterministic results: 1) may lead to improper classification of potential damage when the deterministic results are close to the damage thresholds, and 2) provide relatively little information on the level of confidence in the predicted result. Finally, note that the input uncertainty in the analysis of SAM and ChiFXWS is small because both SAM and ChiFXWS are valuable buildings and their underground conditions and building lay-outs were well surveyed. In practice, even larger uncertainty may exist, which will lead to a wider empirical CDF.

7. Conclusions

In this paper, a two-stage elastoplastic procedure to simulate soil-structure-interaction is applied to assess building damage caused by braced deep excavations. In the first stage, the KJHH and KSJH models by Kung et al. (2007) and Schuster et al. (2009) are employed to develop a new continuous equation to describe the greenfield ground

displacement induced by excavation works. In the second stage, the building deformation is determined through a soil-structure-interaction analysis. This two-stage approach is integrated into the computer program ASRE, which was originally created by Franza and DeJong (2019). This paper also contributes a more functional 2D elastic frame structural analysis model in order to analyze separate footings, infill walls, and frame members with different dimensions and materials.

The two-stage soil-structure-interaction procedure is applied to two case studies and the uncertainty in the case studies are analyzed. For both case studies, the uncertainty related to the ground displacement estimation is the major source of uncertainty in building damage assessment. When the building is modeled as an equivalent beam, the building analysis method also contributes a considerable amount of uncertainty to building damage assessment, while the model of a 2D elastic frame has a much smaller contribution to the damage assessment uncertainty. This implies that future studies on better estimation of ground displacement may be critical to provide a more reliable early stage damage assessment.

A probabilistic analysis approach is proposed to quantify the uncertainty of early-stage damage assessment results. This approach helps practitioners to quantify simplifications and approximations made in analyses, so that a confidence level of building damage assessment can be determined together with a potential level of damage. If the confidence level of the assessment result of a target building is low, more detailed examinations should be conducted. The proposed probabilistic analysis approach and the SSI analysis program ASRE are integrated into the computer program UQESI.

CRediT authorship contribution statement

Jinyan Zhao: Methodology, Software, Validation, Formal analysis, Investigation, Writing – original draft, Visualization. **Stefan Ritter:** Conceptualization, Methodology, Resources, Writing – review & editing. **Matthew J. DeJong:** Conceptualization, Methodology, Writing – review & editing, Supervision, Project administration, Funding acquisition.

Declaration of Competing Interest

The authors declare that they have no known competing financial interests or personal relationships that could have appeared to influence the work reported in this paper.

Appendixes

Appendix 1:. Semi-empirical structural damage estimation methods

Burland et al. (1978) proposed to evaluate building cracking potential by simplifying buildings as deep isotropic simply supported beams. Both bending and shear deformation are considered and equations to calculate the maximum bending strain ($\varepsilon_{b(max)}$) and maximum diagonal tensile strain ($\varepsilon_{d(max)}$) from deflection ratio ($\frac{\Delta}{L}$) are provided (Eq. (13) and (14)). Eq. (13) and (14) are derived based on the deflection at the middle of a center loaded simply supported Timoshenko beam, where E and G are elastic and shear modulus of the beam, I is the moment of inertia, L is the length of the sagging or hogging beam segment and y is the distance from the extreme fibre to the neutral axis. In sagging deformation, it is assumed that the beam neutral axis is at the mid-height of the beam (i.e., $y = \frac{H}{2}$). In hogging deformation, Burland et al. (1978) assumed that foundations and soil provide significant restraint to the buildings and the neutral axis should be considered at the bottom of the beam (i.e., the extreme fibre is at beam top and $y = H$). The larger of $\varepsilon_{b(max)}$ and $\varepsilon_{d(max)}$ is called critical tensile strain (ε_{crit}) and Burland et al. (1978) suggested that the average critical tensile strain for the initiation of crack in brickwork is around 0.05%.

$$\varepsilon_{b(max)} = \frac{\Delta}{L}\frac{12y}{L}\frac{1}{1+\frac{18}{L^2}\frac{I}{H}\frac{E}{G}} \tag{13}$$

$$\varepsilon_{d(max)} = \frac{\Delta}{L}\frac{1}{1+\frac{L^2}{18}\frac{H}{I}\frac{G}{E}} \tag{14}$$

Burland et al. (1978)'s method is widely adopted for analysis of bearing wall structures on continuous footings, though there are several deficiencies with this method. First, assuming a bottom neutral axis in hogging deformation mode leads to a large shear stress at the beam bottom, which can not be balanced with the friction between soil and structure (Dalgic et al. (2018)). This implies the importance of modeling the slippage between the soil and the foundation. Second, although this method works well with buildings on continuous footings, it may not be reasonable to model a frame structure on separate footings as a continuous simply supported beam. Finally, Burland et al. (1978)'s method does not consider horizontal strain, which is argued by Boscardin and Cording (1989) to be a significant component of ε_{crit}.

Boscardin and Cording (1989) therefore modified Burland et al. (1978)'s definition of ε_{crit} as Eq. (15) and (16), where ε_h is defined as the change of building length divided by the original building length. $\varepsilon_{b(max)}$ and $\varepsilon_{d(max)}$ can be determined with Eq. (13) and (14). To quantify the level of building damage, Boscardin and Cording (1989) suggested to classify building damage into 5 categories according to the magnitude of ε_{crit}. This criterion is given in Table 1.

Although ε_h is taken into account, Boscardin and Cording (1989) still modeled the entire building as a deep beam and did not consider separate footings. To evaluate the damage of a building that consists of individual units governing its structural response, Son and Cording (2005) updated Boscardin and Cording (1989)'s method based on the state of strain at each building unit. A building unit, as defined by Son and Cording (2005), can be characterized as a section between two columns, two different building geometries or stiffness characteristics and two different ground displacement gradients. Son and Cording (2005) suggested using angular distortion β to compute ε_{crit} instead of using deflection ratio $\frac{\Delta}{L}$ in Burland et al. (1978)'s method. In Son and Cording (2005)'s method, ε_{crit} determined from distortion (β) and horizontal strain (ε_h) with Eq. (9) and (10) is used to classify building damage, where β is defined as settlement difference (slope) minus rigid rotation (tilt) of a building unit (see Fig. 4). Due to a different definition of ε_{crit}, the criterion of building damage categories are also updated and shown in Table 1.

$$\varepsilon_{crit} = \varepsilon_{b(max)} + \varepsilon_h \tag{15}$$

$$\varepsilon_{crit} = \max_{\theta}\left\{\varepsilon_h cos^2\theta + 2\varepsilon_{b(max)} cos\theta sin\theta\right\} \tag{16}$$

Appendix 2:. Sobol's sensitivity analysis

The first order (S_i) and total effect ($S_{T,i}$) Sobol's indices are defined with Eq. (17), where Y is the output of the system being analyzed and X_i is the i_{th} input of the system. $E(Y|X_i))$ means the expectation of Y conditioned on X_i, while $E(Y|X_{\sim i})$ means the expectation of Y conditioned on all the other input parameters except X_i.

$$S_i = \frac{Var_{X_i}(E(Y|X_i))}{Var(Y)}$$
$$S_{T,i} = 1 - \frac{Var_{X_{\sim i}}\left(E\left(Y|X_{\sim i}\right)\right)}{Var(Y)} \tag{17}$$

Because the system being analyzed in this paper (with input listed in Table 3 and building damage level as output) is nonlinear, there is no theoretical method to calculate Sobol's indices. Therefore, the experiment design proposed by Saltelli et al. (2008) is adopted to estimate the Sobol's indices with Monte-Carlo integration. The procedures are:

- Generate two (N, R) sample matrices **A** and **B**, where N is the number of base sample size and R is the number of input parameters. Each row of **A** and **B** corresponds to a group of independent samples of the input parameters. Quasi-random sampling should be adopted to accelerate the convergence of the Monte-Carlo integration.
- Create matrices $\mathbf{C_i}$, where $i = 1, 2, \ldots R$, with the i_{th} column identical to **A** and all other columns identical to **B**.
- Compute the model output $\mathbf{y_A}$, $\mathbf{y_B}$ and $\mathbf{y_{C_i}}$ by evaluating input matrices **A**, **B** and $\mathbf{C_i}$. There are in total $N(R+2)$ model evaluations.
- Calculate the first order and total effect indices with Eq. (18).

The number of base sample N is usually taken as several hundreds to thousands depending on the system being analyzed. To ensure convergence, N is taken as 2048 in this paper, and insignificant changes were observed when N was increased further.

$$S_i = \frac{\frac{1}{N}\sum_{j=1}^{N} y_A{}^{(j)} y_B{}^{(j)} - f_0^2}{\frac{1}{N}\sum_{j=1}^{N} y_A{}^{(j)} y_A{}^{(j)} - f_0^2}$$
$$S_{T,i} = 1 - \frac{\frac{1}{N}\sum_{j=1}^{N} y_B{}^{(j)} y_{C_i}{}^{(j)} - f_0^2}{\frac{1}{N}\sum_{j=1}^{N} y_A{}^{(j)} y_A{}^{(j)} - f_0^2} \tag{18}$$
$$f_0^2 = \left(\sum_{j=1}^{N} y_A{}^{(j)}\right)^2$$

References

Amorosi, A., d Boldini, D., De Felice, G., Malena, M., Sebastianelli, M., 2014. Tunnelling-Induced Deformation and Damage on Historical Masonry Structures. Géotechnique 64 (2), 118–130.

Ayyub, B.M., Klir, G.J., 2006. Uncertainty Modeling and Analysis in Engineering and the Sciences. CRC Press.

Baecher, G.B., Christian, J.T., 2005. Reliability and Statistics in Geotechnical Engineering. John Wiley & Sons.

Boldini, Daniela, Losacco, Nunzio, Bertolin, Sara, Amorosi, Angelo, 2018. Finite Element Modelling of Tunnelling-Induced Displacements on Framed Structures. Tunn. Undergr. Space Technol. 80, 222–231.

Boscardin, Marco D., Cording, Edward J., 1989. Building Response to Excavation-Induced Settlement. J. Geotech. Eng. 115 (1), 1–21.

Burland, J.B., Broms, B.B., De Mello, V.FB., 1978. Behaviour of Foundations and Structures. Build. Res. Establish. Garston.

Dalgic, Korhan Deniz, Hendriks, Max A.N., Ilki, Alper, 2018. Building Response to Tunnelling-and Excavation-Induced Ground Movements: Using Transfer Functions to Review the Limiting Tensile Strain Method. Struct. Infrastruct. Eng. 14 (6), 766–779.

Dimmock, Paul Simon, Mair, Robert James, 2008. Effect of Building Stiffness on Tunnelling-Induced Ground Movement. Tunn. Undergr. Space Technol. 23 (4), 438–450.

Edeling, Wouter, Arabnejad, Hamid, Sinclair, Robbie, Suleimenova, Diana, Gopalakrishnan, Krishnakumar, Bosak, Bartosz, Groen, Derek, Mahmood, Imran, Crommelin, Daan, Coveney, Peter V., 2021. The Impact of Uncertainty on Predictions of the Covidsim Epidemiological Code. Nat. Comput. Sci. 1 (2), 128–135.

Elkayam, Itai, Klar, Assaf, 2019. Nonlinear Elastoplastic Formulation for Tunneling Effects on Superstructures. Can. Geotech. J. 56 (7), 956–969.

Fargnoli, V., Gragnano, C.G., Boldini, D., Amorosi, A., 2015. 3D Numerical Modelling of Soil-Structure Interaction During Epb Tunnelling. Géotechnique 65 (1), 23–37.

Fema, 1998. Evaluation of Earthquake Damaged Concrete and Masonry Wall Buildings: Basic Procedures Manual. In: FEMA 306: Prestandard and Commentary for the Seismic Rehabilitation of Buildings, p. 250.

Finno, Richard J., Sebastian, L., Bryson, 2002. Response of Building Adjacent to Stiff Excavation Support System in Soft Clay. J. Perform. Constr. Facil 16 (1), 10–20.

Finno, Richard J., Voss Jr, Frank T., Rossow, Edwin, Tanner Blackburn, J., 2005. Evaluating Damage Potential in Buildings Affected by Excavations. J. Geotech. Geoenviron. Eng. 131 (10), 1199–1210.

Franza, Andrea, Acikgoz, Sinan, DeJong, Matthew J., 2020a. Timoshenko Beam Models for the Coupled Analysis of Building Response to Tunnelling. Tunn. Undergr. Space Technol. 96, 103160.

Franza, Andrea, DeJong, Matthew J., 2019. Elastoplastic Solutions to Predict Tunneling-Induced Load Redistribution and Deformation of Surface Structures. J. Geotech. Geoenviron. Eng. 145 (4), 04019007.

Franza, Andrea, Ritter, Stefan, Dejong, Matthew J., 2020b. Continuum Solutions for Tunnel-Building Interaction and a Modified Framework for Deformation Prediction. Géotechnique 70 (2), 108–122.

Franzius, J.N., Potts, D.M., Burland, J.B., 2006. The Response of Surface Structures to Tunnel Construction. Proc. Inst. Civil Eng.-Geotech. Eng. 159 (1), 3–17.

Ghobarah, A., 2004. On Drift Limits Associated with Different Damage Levels. International Workshop on Performance-Based Seismic Design. Dept. of Civil Engineering, McMaster University.

Giardina, Giorgia, DeJong, Matthew J., Chalmers, Benjamin, Ormond, Bryan, Mair, Robert J., 2018. A Comparison of Current Analytical Methods for Predicting Soil-Structure Interaction Due to Tunnelling. Tunn. Undergr. Space Technol. 79, 319–335.

Giardina, G., Losacco, N., DeJong, M.J., Viggiani, G.MB., Mair, R.J., 2020. Effect of Soil Models on the Prediction of Tunnelling-Induced Deformations of Structures. Proc. Inst. Civil Eng.-Geotech. Eng. 173 (5), 379–397.

Giardina, Giorgia, Van de Graaf, Anne V., Hendriks, Max A.N., Rots, Jan G., Marini, Alessandra, 2013. Numerical Analysis of a Masonry Façade Subject to Tunnelling-Induced Settlements. Eng. Struct. 54, 234–247.

Goh, K.H., Mair, R.J., 2011. Building Damage Assessment for Deep Excavations in Singapore and the Influence of Building Stiffness. Geotech. Eng. 42, 1–12.

Hsieh, Pio-Go, Chang-Yu, Ou, 1998. Shape of Ground Surface Settlement Profiles Caused by Excavation. Can. Geotech. J. 35 (6), 1004–1017.

Klar, A., Vorster, T.E., Soga, Kenichi, Mair, R.J., 2007. Elastoplastic Solution for Soil-Pipe-Tunnel Interaction. J. Geotech. Geoenviron. Eng. 133 (7), 782–792.

Kung, Gordon T., Hsein Juang, C., Hsiao, Evan C., Hashash, Youssef M., 2007. Simplified Model for Wall Deflection and Ground-Surface Settlement Caused by Braced Excavation in Clays. J. Geotech. Geoenviron. Eng. 133 (6), 731–747.

Mair, R., 2013. Tunnelling and Deep Excavations: Ground Movements and Their Effects. In: Proceedings of the 15th European Conference on Soil Mechanics and Geotechnical Engineering–Geotechnics of Hard Soils–Weak Rocks (Part 4). IOS Press, Athens, Greece, pp. 39–70.

Mair, R.J., Taylor, R.N., Burland, J.B., 1996. Prediction of Ground Movements and Assessment of Risk of Building Damage Due to Bored Tunnelling. In: *Geotechnical Aspects of Underground Construction in Soft Ground*, pp. 713–718.

Potts, D.M., Addenbrooke, T.I., 1997. A Structure's Influence on Tunnelling-Induced Ground Movements. Proc. Inst. Civil Eng.-Geotech. Eng. 125 (2), 109–125.

Saltelli, Andrea, Annoni, Paola, Azzini, Ivano, Campolongo, Francesca, Ratto, Marco, Tarantola, Stefano, 2010. Variance Based Sensitivity Analysis of Model Output. Design and Estimator for the Total Sensitivity Index. Comput. Phys. Commun. 181 (2), 259–270.

Saltelli, A., Ratto, M., Andres, T., Campolongo, F., Cariboni, J., Gatelli, D., Saisana, M., Tarantola, Stefano, 2008. Global Sensitivity Analysis: The Primer. John Wiley & Sons.

Schuster, Matt, Kung, Gordon Tung-Chin, Hsein Juang, C., Hashash, Youssef M.A., 2009. Simplified Model for Evaluating Damage Potential of Buildings Adjacent to a Braced Excavation. J. Geotech. Geoenviron. Eng. 135 (12), 1823–1835.

Son, Moorak, Cording, Edward J., 2005. Estimation of Building Damage Due to Excavation-Induced Ground Movements. J. Geotech. Geoenviron. Eng. 131 (2), 162–177.

Son, Moorak, Cording, Edward J., 2007. Evaluation of Building Stiffness for Building Response Analysis to Excavation-Induced Ground Movements. J. Geotech. Geoenviron. Eng. 133 (8), 995–1002.

Vaziri, H., Simpson, B., Pappin, J.W., Simpson, L., 1982. Integrated Forms of Mindlin's Equations. Géotechnique 32 (3), 275–278.

Yiu, W.N., Burd, H.J., Martin, C.M., 2017. Finite-Element Modelling for the Assessment of Tunnel-Induced Damage to a Masonry Building. Géotechnique 67 (9), 780–794.

Zhao, Jinyan, Franza, Andrea, DeJong, Matthew J., 2021. Method for Probabilistic Assessment of Tunneling-Induced Damage to Surface Structures Considering Soil-Structure Interaction Effects. ASCE-ASME J. Risk Uncerta. Eng. Syst., A: Civil Eng. 7 (4), 04021055.